# Effects of a Weak Transverse Magnetic Field and a Spatial Potential on Negative Ion Transport in Negative Ion Sources

T.Sakurabayashi, A.Hatayama and M.Bacal*

*Faculty of Science and Technology, Keio Univ., Hiyoshi, Yokohama 223-8522, Japan*

**Laboratoire de Physique et Technologie des Plasmas, Ecole Polytechnique, Laboratoire du CRNS, 91128 Palaisseau Cedex, France*

**Abstract.**

The effects of the weak magnetic field on the negative ion ($H^-$) extraction in a negative ion source have been studied by means of a two-dimensional electrostatic particle simulation. A particle-in-cell (PIC) model is used which simulates the motion of the charged particles in their self-consistent electric field. Since most electrons are magnetized by the weak magnetic field, it is shown that more $H^-$ ions arrive instead of electrons in the region close to the plasma grid in order to ensure the plasma neutrality. In the present article, the effect of the electron diffusion across the weak magnetic field is also taken into account. Although the electron diffusion effects weaken the difference of the dynamics between electrons and $H^+$ ions, the presence of the magnetic field still has a large contribution to the enhancement of the $H^-$ extraction.

## Ⅰ. INTRODUCTION

Neutral beam injection based on the negative ion beam is one of the most promising candidates for heating and current drive in future fusion reactors. To generate intense beams of negative ions and optimize the negative ion source[1-3], understanding of the transport properties of negative ions ($H^-$)[4-7] is indispensable.

In the experiments, the extraction of $H^-$ ions has been significantly improved by the weak magnetic field[8-9]. The electrode of the extractor in contact with the plasma has a pair of magnets as shown in Fig.1. The magnets create a transverse magnetic field in the extractor which is strong enough to suppress electrons from the negative ion beam. In addition, electrons inside the plasma source near the PG can be easily magnetized by the stray field of this electron suppression magnet (a few tens of Gauss) and lost along the field line, while

positive ions ($H^+$) cannot be magnetized because of the larger Larmor radius. This difference in dynamics between electrons and $H^+$ ions perturbs the plasma neutrality in this region and leads to the formation of a positive electric potential. This modification in the plasma neutrality and resultant electric potential due to the weak magnetic field are considered to be very important for the $H^-$ ion transport and extraction.

In our previous paper[10], the idea that more $H^-$ ions arrive in the region close to the PG in order to ensure the plasma neutrality was confirmed by the PIC simulation. However, the effect of the electron diffusion across the weak magnetic field has not been taken into account. In Ref.[11], preliminary study was done with the effect of electron diffusion. The electron diffusion had little effects on the $H^-$ transport because most of the electrons were lost along the field line before they diffused across the weak magnetic field.

However, in Ref.[10, 11], we neglected the variation of magnetic field along the field line for simplicity. In the realistic geometry, the magnetic field is stronger near the electron suppression magnets in Fig.1. If we take into account this effect, some electrons may move back and forth along the field line due to the effect of magnetic mirror. Owing to this effect of magnetic mirror, the effective loss time along the field line could become large. Electrons trapped between the magnetic mirrors could have enough time to diffuse across the magnetic field before they are lost along the field line. Thus, in order to perform a more realistic simulation, further analysis incorporating both the effects of (i) the variation of magnetic field and (ii) the collision processes is required.

In this paper, we take into these two effects for overall understanding of the effect of weak magnetic field on the spatial structure of electric potential and on the resultant $H^-$ transport under more realistic model.

## Ⅱ. SIMULATION MODEL

The motion of the charged particles ($H^-$ ions, $H^+$ ions and electrons) in their self-consistent electric field is calculated by the PIC method[12-15]. The trajectories of the particles are calculated by numerically solving the equation of motion,

$$m_s \, d\mathbf{v}/dt = q_s(\mathbf{E} + \mathbf{v}\times\mathbf{B}), \qquad (1)$$

where $m_s$, $\mathbf{v}$, $q_s$, $\mathbf{E}$ and $\mathbf{B}$ are the charged particle mass, velocity, charge, electric field and magnetic field for particles of species $s$, respectively. To obtain the charge density on a grid point, the particle charge is assigned to each grid point by linear interpolation. The particle densities ($n_s$) also are calculated from the charge densities on the grid points. Poisson's equation for the spatial electric potential $\phi$,

$$\nabla^2\phi = -q(n_{H^+} - n_e - n_{H^-})/\varepsilon_0 , \qquad (2)$$

is solved by the finite difference method, where $\varepsilon_0$ is the permittivity of free space. The numerical algorithm employed to solve Poisson's equation is the SIP (Stone's Strongly Implicit Procedure) method[16].

The extractor used in the experiments consists of three electrodes, a plasma grid (PG), an extraction grid (EG) and an acceleration grid (AG), as shown in Fig.1 (a). The electrodes have an extraction aperture. A pair of magnets creating the weak magnetic field near the PG is located in the EG.

The magnets are installed in parallel on both sides of the extraction aperture as schematically shown in Fig.1 (b). The resultant magnetic lines of force are also shown in Fig.1 (b) with broken lines. We mainly focus on the limited region around the extraction aperture in this simulation. The coordinate system used in the analysis is also shown in Fig.1 (b). We assume a spatial uniformity in the $z$-direction near the extraction aperture, because the lengths of the magnets are relatively long in comparison with the extraction aperture and the edge effect of the magnetic field in the $z$-direction can be neglected. We therefore now confine our attention to the two-dimensional spatial profiles in the $x-y$ plane in Fig.1 (b).

The model geometry in the simulation is shown in Fig.2 by including only the PG and EG. The weak magnetic field exists over the entire modeled region. In our previous study [10-11], relatively a simple model for the magnetic field is employed. The magnetic field component was assumed to be only in the $y$-direction, namely $B_y$. A simple analytic expression with the Gaussian profile in the $x$-direction was used. As was pointed out in Sec.I, the variation of the magnetic field along the field line and the resultant magnetic mirror effect are considered to be important for electron diffusion. For this purpose, in this study, a pair of magnets with the infinite length in the $z$-direction is installed in the model geometry as shown in Fig.2. The magnetic filed has both components $B_x$ and $B_y$ in the present model. Figure 3 shows the spatial profile of the strength of magnetic field $B = \sqrt{B_x^2 + B_y^2}$. The magnetic field at each point is calculated by using the analytical solution based on the magnetic charge model[17].

Electron diffusion across the weak magnetic field is taken into account by Monte-Carlo method in the following manner. For each time step of integration, to judge if the collision event takes place or not, the path length estimator algorithm[18] has been employed. The probability for electrons to collide with $H^+$ ions and neutrals is estimated as $P_e = 1 - \exp(-\sum \nu_e^{tot} \Delta t)$. Here, $\Delta t$ is the time step of integration and $\nu_e^{tot}$ is the total collision frequency of electrons including two kinds of collisions, electron-neutral and electron-ion collisions; $\nu_e^{tot} = \nu_{en} + \nu_{ei}$. Electron-electron collisions are neglected, since like

particle collisions are not important for the spatial diffusion across the magnetic field. The electron speed $v_e$ is assumed to be almost unchanged before and after collision because of large mass difference in electron-neutral and electron-ion collisions. If once the collision event takes place, then the scattering angles $\theta$ and $\phi$ are chosen randomly from an isotopic distribution. The Monte Carlo collision model employed here is relatively simple. For example, it does not take into account the small scattering feature of Coulomb scattering, i.e., electron-ion collision. However, at least, as far as the diffusion in the uniform *B*-field with $\left(\omega_c / \nu_e^{tot}\right)^2 >> 1$ is concerned, this model gives the same result of a particle diffusion coefficient $D_\perp = r_L^2 \nu_e^{tot}$ as that obtained from the fluid model, where $\omega_c$ and $r_L$ are the cyclotron frequency and Larmor radius, respectively.

The initial condition of the calculation region is an empty computation region. Let the left-hand boundary ($x = 0$) be the upstream boundary; we call this boundary 'Plasma Line (PL)', shown in Fig.2. The plasma ($x < 0$) is assumed to contain sources which maintain the plasma neutrality and stationary particle fluxes across the PL. Thus the electric field at the PL is zero and equal numbers of positively and negatively charged particles per time step are injected into the calculation region from the PL. The boundary conditions for the particle flux ($\Gamma$) are $\Gamma_{H^+} = \Gamma^-$, $\Gamma^- \equiv \Gamma_e + \Gamma_{H^-}$ and $\Gamma_{H^-} / \Gamma^- = 0.1$, where $\Gamma_{H^+}$, $\Gamma_e$ and $\Gamma_{H^-}$ are the $H^+$ ion flux, the electron flux and the $H^-$ ion flux, respectively. The charged particles are launched isotropically from the PL in the $x$-direction. The initial velocity distribution is a Maxwellian distribution with temperatures $T_e = 1.0$ eV, $T_{H^+} = 0.5$ eV, $T_{H^-} = 0.5$ eV . If particles cross the PL from right to left, they are reloaded with new velocities in addition to the particles successively injected per time step. As shown in Fig.2, the wall at $x = 4$ cm is used as the PG, which has an extraction aperture of 1 cm. The PG and wall potentials are fixed ($\phi = 0$). The particles reaching the PG or walls are removed from the calculation region. The wall at $x = 5$ cm is used as EG, which is the right-hand boundary and has no extraction aperture. The conditions are the same as those for the walls and the PG except for the EG potential ($\phi_{EG}$). As was discussed in Ref.[10,11], we have adjusted $\phi_{EG}$ to an appropriate value ($\phi_{EG} = 10$ V) in order to separate the pure effect of the transverse magnetic field from the penetration effect of the EG voltage on the $H^-$ extraction.

## Ⅲ. SIMULATION RESULTS

In order to study the effects of a weak transverse magnetic field and electron diffusion across the field on $H^-$ extraction, the following three cases are compared;

case (A)- without both effects of the magnetic field and electron diffusion,

case (B)- with only the effect of the weak magnetic field and

case (C)- with both effects of the weak magnetic field and electron diffusion.

Except for these effects, other conditions are the same as those in Sec.II for these three cases.

Figure 4 (a), (b) and (c) show the time evolution of calculated electrostatic potentials for each point along the LINE shown in Fig.4(d). Figure 4 (a), (b) and (c) are the results for case (A), (B) and (C), respectively. After about $5\times10^5$ time steps, quasi-steady states have been reached for all the cases as seen from Fig.4.

Under these quasi-steady state conditions, the density profiles of $H^+$ ions, electrons and $H^-$ ions are compared for case (A), (B) and (C). In Fig.5, the density profiles are plotted versus the distance along the LINE shown in Fig.4(d) for each case. The densities are normalized by the first cell $H^+$ density.

As in Ref.[10], the extraction of $H^-$ ions for case (B) is significantly enhanced in comparison with case (A). Also, for case (C), significant increase of $H^-$ extraction compared with case (A) has been observed in the simulation. Due to the diffusion across the magnetic field, electron diffusion has a effect to weaken the trapping effect by the magnetic field. However, the enhancement factor of $H^-$ current for case (C) has been about the same as that for case (B). To understand these features and the physical mechanism of the enhancement of the $H^-$ extraction for both cases, we will make more detailed comparisons of the numerical results in the following subsections.

**Comparison between collisionless cases**

To understand the pure and intrinsic effect of the weak magnetic field on the $H^-$ transport, first we will make a comparison between two cases without the effect of electron diffusion, i.e., case (A) and case (B) in Fig.5. The comparison is useful as a basis for the understanding of the effect of electron diffusion discussed later in the next subsection.

The weak magnetic field drastically affects the density profiles of each species as seen from the comparison between Fig.5(a) and Fig.5(b). For case (B), electrons are magnetized by the magnetic field due to their small Larmor radius. Consequently, most of electrons are localized near the PL as shown in Fig.5(b). Thus, the computational domain can be divided into the following two characteristic regions: the ‘Electron trapping region’, the region from the PL to $x \simeq 1$ cm and the ‘Effective extraction region’, the region from the right-hand side of the ‘Electron trapping region’ to the PG ($1\ \text{cm} \le x \le 4\ \text{cm}$). In the effective extraction region, electron density $n_e$ is almost zero, while $H^+$ density $n_{H^+}$ is comparable to $H^-$ density

$n_{H^-}$. Negative ions are balanced with $H^+$ ions instead of electrons to maintain plasma neutrality.

The weak magnetic filed also affects the spatial structure of the electric potential. Figure 6 shows the potential profiles for (a) without and (b) with the weak magnetic field, respectively. Here, in Fig.6 (a) and (b), we concentrate on the region $0\ \text{cm} \le x \le 3.5\ \text{cm}$ in order to see the difference between these two cases more clearly. As seen from Fig.6 (b), the potential has a characteristic positive peak at $x \approx 1\ \text{cm}$ for case (B) with the week magnetic field, while there exists no such a positive potential peak for case (A). Due to the effect of week magnetic field, the spatial potential changes its spatial structure in such a way that it collects $H^-$ ions. As a result, the $H^-$ density in the effective extraction region increases as shown in Fig.5(b).

The formation process of the potential peak has been already discussed in Ref.[10]. Here, we briefly summarize the main points. Electrons are magnetized by the weak magnetic field and localized in the electron trapping region. Then, a transverse electric field perpendicular to the magnetic field sets up to retard ion motion in the $x$-direction. In order to balance with electrons in the 'electron trapping region', some ions are attracted toward the PL by the transverse electric field, and some ions which have large velocity continue moving towards the PG. As a result, the magnetic field produces two $H^+$ ion flows, i.e., back flow toward PL and the forward flow toward PG. The $H^-$ ions collected in the effective extraction region move together with $H^+$ ions to ensure the plasma neutrality and reach the PG. The position of the potential peak is almost coincident with the point where the H+ ion flows stagnate. Thus, the $H^-$ ions collected in the effective extraction region move together with $H^+$ ions to ensure the plasma neutrality and reach the PG.

**Effects of the electron diffusion across the magnetic field**

To understand the effects of electron diffusion, now we are coming back to Fig.5. As seen from the comparison between Fig.5(b) and Fig.5(c), the density profiles of each species (electrons, $H^+$ ion and $H^-$ ion) are greatly changed by including the effect of electron diffusion.

For case (B) without electron diffusion, electrons never enter the region close to the PG as shown in Fig.5(b). On the other hand, for case (C), electrons diffuse out of the 'electron trapping region' and enter the 'effective extraction region' due to the diffusion across the magnetic filed as shown in Fig.5(c). As a result, the density profiles in Fig.5(c) for electrons and $H^+$ ions are more similar to those for case (A) without the magnetic filed in Fig.5(a) than those for case (B) with the magnetic filed in Fig.5(b).

However, even if the effect of the electron diffusion is taken into account, still relatively a large amount of $H^-$ ions reaches the region close to PG for case (C) than case (A). Consequently, not only electrons, but also $H^-$ ions play a important role to maintain the plasma neutrality near the PG for case(C).

Figure 7 shows a comparison of $H^-$ density among case (A), (B) and (C). The negative ion densities are normalized by the $H^-$ density in the first cell for case (C). In the region $1\,\mathrm{cm} \le x \le 3\,\mathrm{cm}$, the $H^-$ density for case (B) becomes larger compared with other cases. However, if we concentrate on the region near the PG ($3\,\mathrm{cm} \le x \le 4\,\mathrm{cm}$), $n_{H^-}$ for case (C) with the electron diffusion is comparable to case (B), or even slightly larger than that for case (B). The extraction current $I_{H^-}$ ($I_{H^-}$:the $H^-$ current that passes through the extraction aperture in Fig.2) for case (C) is comparable to case (B).

These characteristic features of $H^-$ density and extraction current are closely related to the spatial structure of the electric potential. For case (B), electric potential has a peak at around $x \approx 1\,\mathrm{cm}$ as shown in Fig.6(b). As was discussed in the previous subsection and also in Ref.[10], the positive potential peak collects $H^-$ ions from the electron trapping region into the effective extraction region. Injected $H^-$ ions are accelerated into the region to the left of potential peak. After that, they are decelerated in the right of the potential peak. As a result, $n_{H^-}$ becomes relatively large near the potential peak around $1\,\mathrm{cm} \le x \le 2\,\mathrm{cm}$ for case (B) as shown in Fig.7.

On the other hand, no such a clear potential peak at $x \approx 1\,\mathrm{cm}$ was observed in the simulation for case (C) due to the effect of the electron diffusion across the magnetic field. As a result, $n_{H^-}$ for case (C) in the region $1\,\mathrm{cm} \le x \le 2\,\mathrm{cm}$ becomes small compared with case (B) as shown in Fig.7. Instead, for case (C), relatively small positive potential peak can be seen more close to the PG (at $x \approx 3\,\mathrm{cm}$) as shown in Fig.8. Due to this positive potential peak close to the PG, the negative ion density for case (C) becomes comparable to case (B) or even slightly larger in this region ($3\mathrm{cm} < x \le 4\mathrm{cm}$) in front of PG as shown in Fig.7.

Figure 9 shows a typical snap shot of the phase space $(x, v_x)$ plot of each $H^+$ ion, i.e., distribution of the $x$ component of velocity $v_x$ for $H^+$ ions along the LINE in Fig.4(d). Figure 9(a) and (b) correspond to the results for case (B) and case (C), respectively. As was pointed out in the previous subsection, for case (B), a clear back flow of $H^+$ ions arises with negative velocities ($v_x < 0$) toward the PL, where the positive potential peak exists as shown in Fig.6(b). On the other hand, for case (C), no such a clear back flow toward the PL is observed at $x \approx 1\mathrm{cm}$. However, if we focus our attention to the region $2.5\mathrm{cm} < x < 3.5\mathrm{cm}$, a clear retardation of $H^+$ ions is observed around $x \approx 3\,\mathrm{cm}$ as shown in Fig.9(b). The position is almost coincident with the location of the potential peak $x \approx 3\,\mathrm{cm}$ in Fig.8. This modification of potential structure plays a important role to understand the increase in the $H^-$ density in front of the PG in Fig.7 for case (C).

## Ⅳ. SUMMARY

The effect of the weak transverse magnetic field on the $H^-$ extraction in the negative ion source were studied by a 2D PIC simulation. In the present paper, electron diffusion across the magnetic field is taken into account.

Without the effect of the electron diffusion, electrons are magnetized by the magnetic field and localized in the electron trapping region. On the other hand, positive ions ($H^+$) cannot be magnetized due to their large mass. This difference in dynamics between electrons and $H^+$ ions has been verified to lead to the formation of the positive potential peak near the edge of the electron trapping region. The $H^-$ ions are collected by the positive potential peak and move together with $H^+$ ions towards the PG to ensure the plasma neutrality.

With the effect of electron diffusion, both diffused electrons and negative ions are balanced with $H^+$ ions to maintain the plasma neutrality. As a result, the positive potential peak becomes smaller, but it moves closer to PG. Due to this positive potential peak close to the PG, the negative ion density becomes still comparable to the case without electron diffusion, or even slightly larger in front of PG. Consequently, even if we take into account the effect of electron diffusion across the magnetic field, the presence of magnetic field has a large contribution to the enhancement of the $H^-$ extraction.

From these results, the intrinsic physical mechanism of the enhancement of $H^-$ extraction observed in the simulation is possibly explained by the modification of plasma charge neutrality due to the weak transverse magnetic field and the formation of positive potential peak near the PG.

## REFFERENCES


[1] M.Bacal, C.Michaut, L.I.Elizarov, and F.El Balghiti, Rev.Sci.Instrum. **67**, 1138(1996).

[2] C.Courteile, J.Bruneteau, and M.Bacal, Rev.Sci.Instrum. **66**, 2533(1995).

[3] F.El Balghiti-Sube, F.G.Baksht, and M.Bacal, Rev.Sci.Instrum. **67**, 2221(1996).

[4] T.Sakurabayashi, A.Hatayama, K.Miyamoto, M.Ogasawara, and M.Bacal, Rev.Sci.Instrum. **73**, 1048(2002).

[5] M.Uematsu, T.Morishita, A.Hatayama, and T. Sakurabayashi, Rev.Sci.Instrum. **71**, 883(2000).

[6] A.Hatayama, T.Sakurabayashi, Y.Ishii, K.Makino, M.Ogasawara and M.Bacal, Rev.Sci.Instrum. **73**, 910(2002).

[7] K.Makino, T.Sakurabayashi, A.Hatayama, K.Miyamot, M.Ogasawara, Rev.Sci.Instrum. **73**, 1051(2002).

[8] M.Bacal, J.Bruneteau, and P.Devynck, Rev.Sci.Instrum. **59**, 2152(1988).

[9] P.Devynck, M.Bacal, J.Bruneteau, and F. Hillion, Revue Phys.Appl. (Paris) **22**, 753(1987).

[10] T.Sakurabayashi, A.Hatayama and M.Bacal, J.Appl.Phys. **95**, 3937(2004).

[11] T.Sakurabayashi, A.Hatayama and M.Bacal, Rev.Sci.Instrum. **75**, 1770 (2004).

[12] C.K.Birdsall and A.B.Langdon, *Plasma Physics via Computer Simulation* (McGraw-Hill, New York, 1985).

[13] J.P.Verboncoeur, M.V.Alves, V.Vahedi and C..K.Birdsall, J.Comp.Phys. **104**, 321(1993).

[14] W.S.Lawson, J.Comp.Phys. **80**, 253(1989).

[15] R.J.Procassini, C.K.Birdsall, and E.C.Morse, Phys.Fluids B **2**, 3191(1990).

[16] H.L.Stone, SIAM J.Numer.Anal. **5**, 530(1968).

[17] Y.Ohara, M.Akiba, H.Horiike, H.Imai, Y.Okumura and S.Tanaka, J.Appl.Phys. **61**, 1323(1987).

[18] M.H.Hughes and D.E.Post, J.Comp.Phys. **28**, 43(1978).

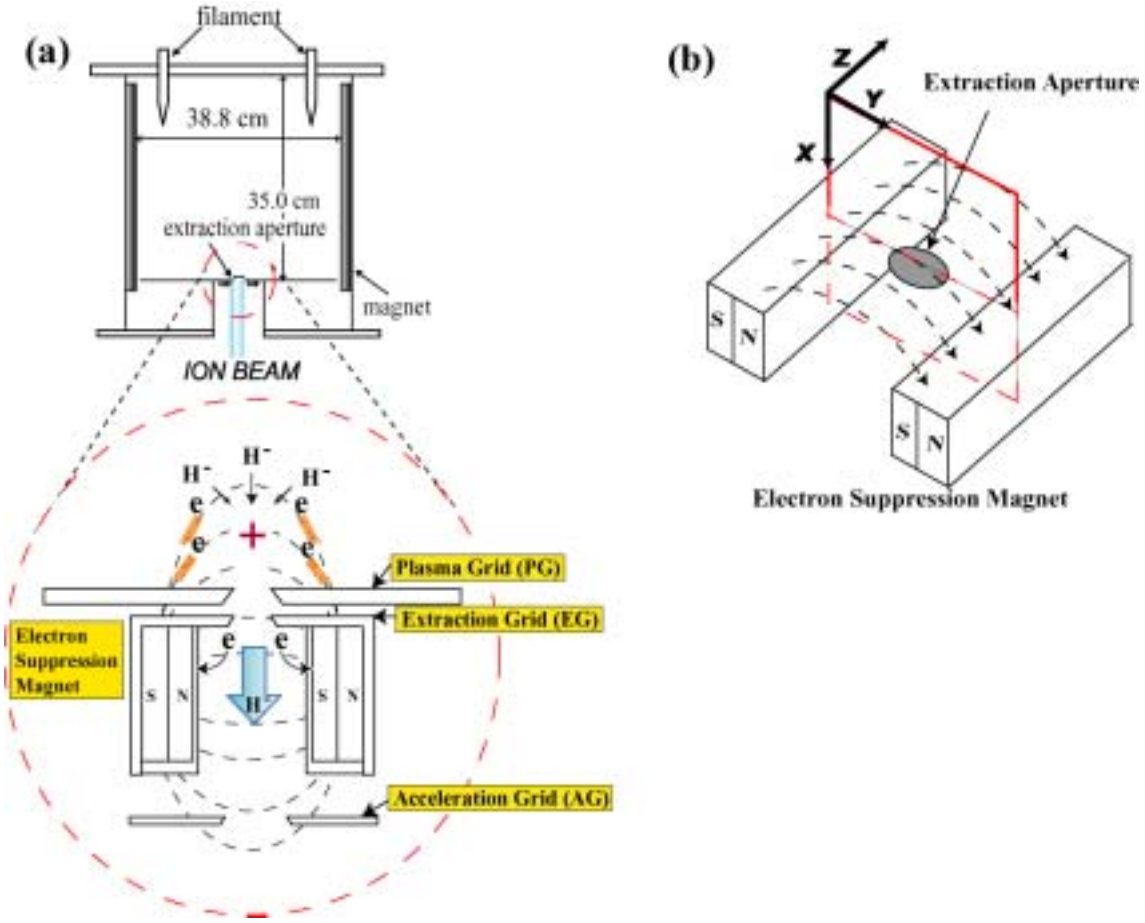


Fig.1 Schematic diagram of the negative ion source. (a) cross-sectional view with the enlargement of the extractor. The electrodes of the extraction system have three electrodes, (PG, EG and AG) and a pair of magnets create the weak magnetic field. (b) bird's–eye view of a pair of magnets. Magnetic lines of force are denoted by broken lines.

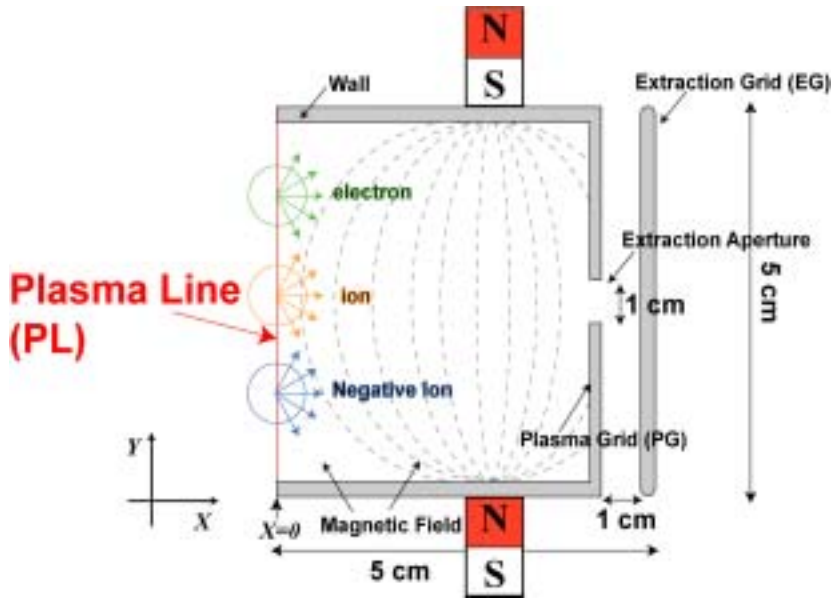


Fig.2 Schematic diagram of 2D particle simulation model used in this study. The left-hand boundary (PL: $x = 0$ cm ) is the upstream boundary. The wall at $x = 4.0$ cm is used as PG, which has an extraction aperture of $1.0$ cm . The wall at $x = 5.0$ cm is used as EG.

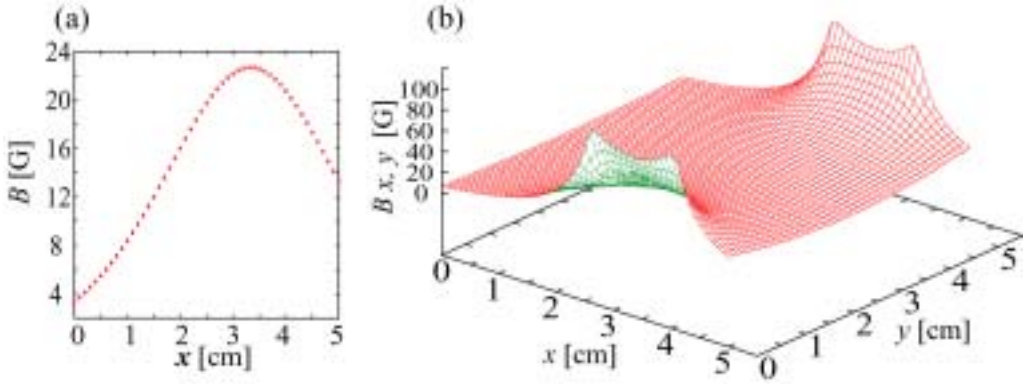


Fig.3 Spatial profile of the weak magnetic field: (a) in the $x$-direction at $y = 2.5$cm and (b) in the $x - y$ plane.

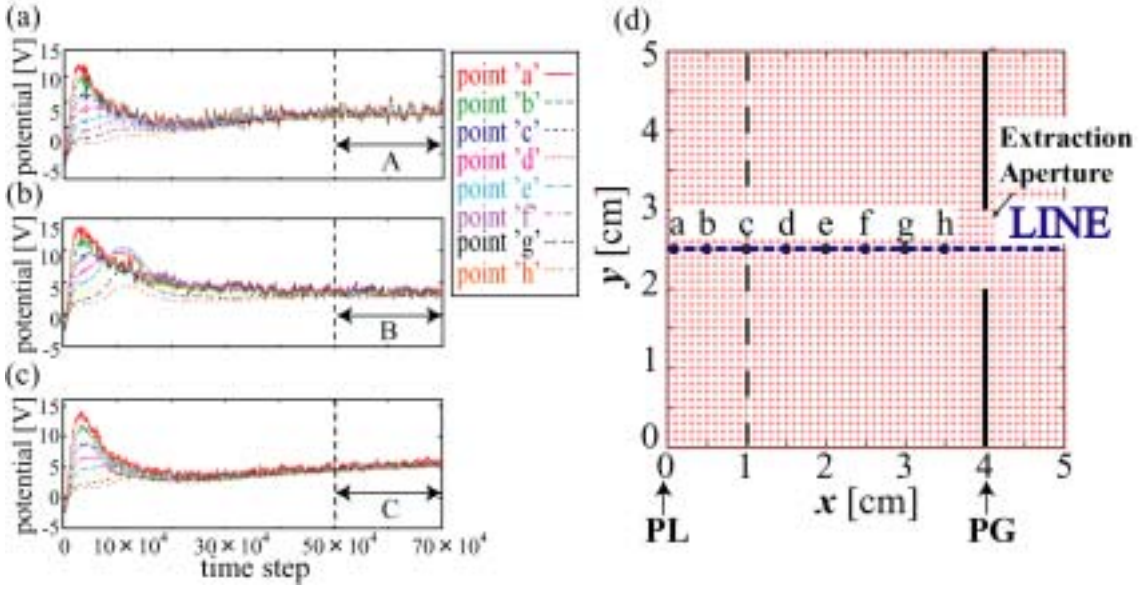


Fig.4 Time evolution of potentials (a) without the magnetic field and diffusion, (b) with only the weak magnetic field and (c) with both effects of the weak magnetic field and electron diffusion at points a~h in (d).

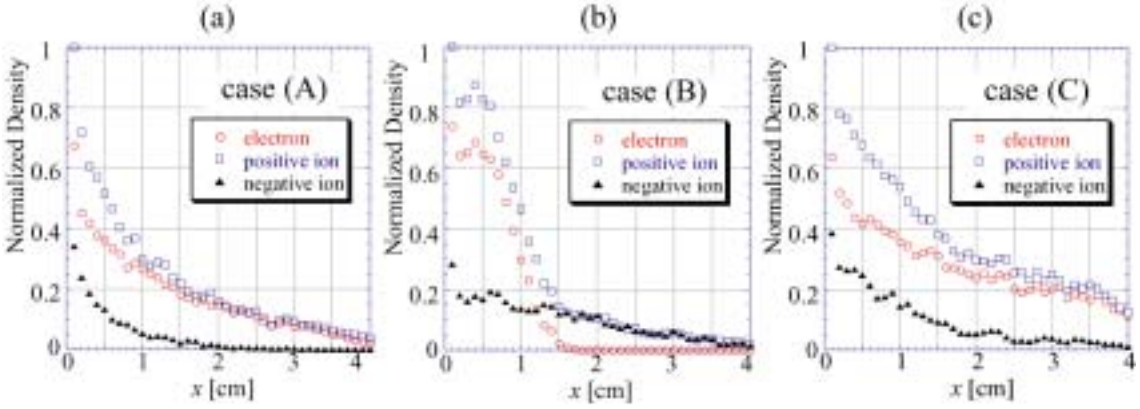


Fig.5 Variation of the charged particle densities versus the axial distance along the LINE shown in Fig.4 (c) for each case. Figure 5 (a), (b) and (c) are the results for case (A), (B) and (C), respectively. For case (A), the charge neutrality is maintained by mainly $H^+$ ions and electrons. For case (B), $H^-$ ions are balanced with $H^+$ ions instead of electrons to maintain the plasma neutrality. For case (C), both negative ions and diffused electrons are balanced with $H^+$ ions near the PG

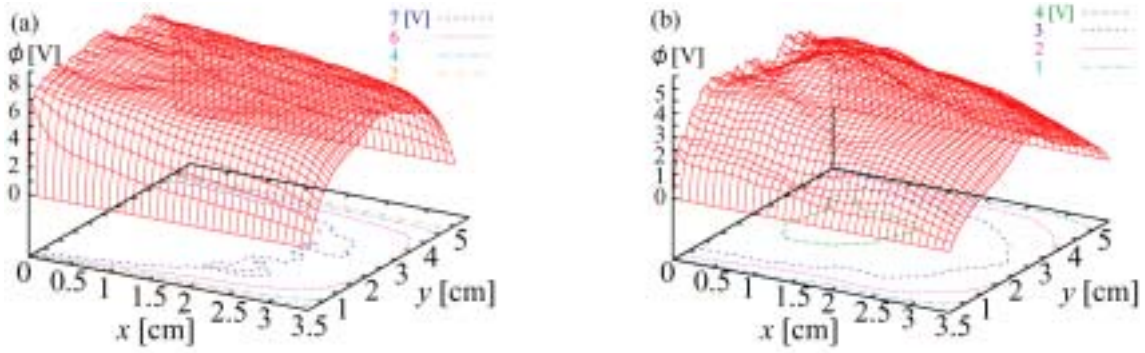


Fig.6 Structure of the potential in the region $0\ \text{cm} \le x \le 3.5\ \text{cm}$ (a) without the weak magnetic field and (b) with the weak magnetic field. The electron diffusion is not taken into account for both cases.

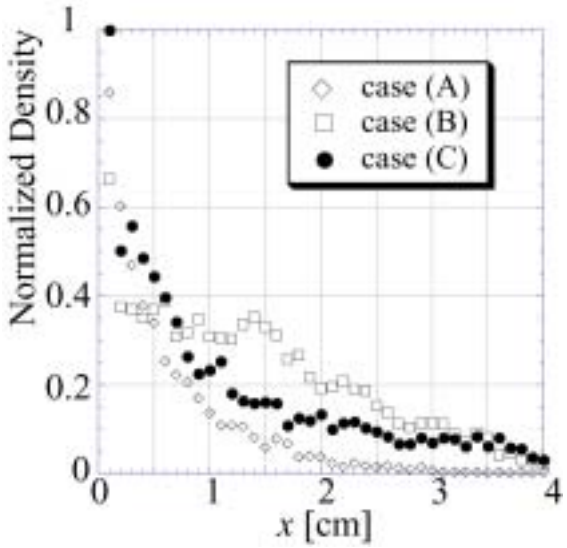


Fig.7 Comparison of spatial profiles of negative ion density among case (A), (B) and (C).

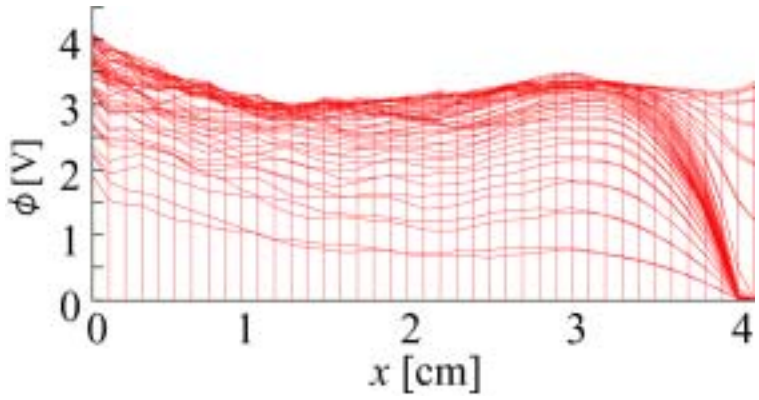


Fig.8 Side view of spatial potential structure in the region $0\ \text{cm} \le x \le 4\ \text{cm}$ for case (C). Relatively a small positive potential peak locates near the PG $x \simeq 3.0\ \text{cm}$.

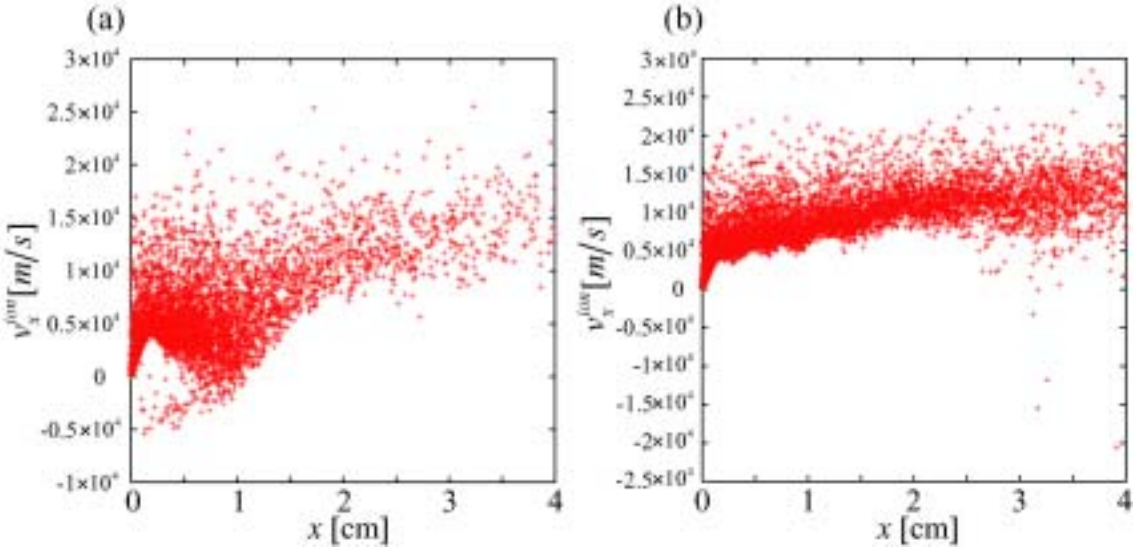


Fig.9 Distribution of $x$ component of ion velocity along the LINE. (a) For case (B), positive ion flow is stagnated at $x \simeq 1\ \text{cm}$. (b) For case (C), some ions are decelerated at $x \simeq 3.0\ \text{cm}$.